



# Data Integration by Fuzzy Logic for Mineral Prospectivity Mapping in Ferdows–Gonabad–Bajestan Belt, Khorasan Razavi Province, Iran

Zohreh Arjmand Lary<sup>1</sup> · Mehdi Honarmand<sup>1</sup>  · Hadi Shahriari<sup>2</sup>  · Mahdieh Hosseinjani Zadeh<sup>1</sup> 

Received: 27 August 2021 / Accepted: 16 April 2024 / Published online: 15 May 2024  
© Indian Society of Remote Sensing 2024

## Abstract

This research aims to specify the mineral prospects in the Ferdows–Gonabad–Bajestan belt (FGBB), Iran, using fuzzy logic. Geology, geochemistry, and remote sensing data were utilized to produce a mineral prospectivity map (MPM). ASTER images were analyzed using spectral angle mapper (SAM) and linear spectral unmixing (LSU) methods to enhance hydrothermal alterations. The faults were derived from Sentinel-2A and SPOT5 images. Weighted maps of the intersection of faults and intrusive contacts, proximity to faults, and photolineament factor (PF) were performed to build the geological structures layer. Regional geology and stream sediment geochemistry maps were performed to produce corresponding evidential layers. Four evidential layers including geology, hydrothermal alteration, geological structures, and geochemistry were defined based on the knowledge of experts. Evidential layers were integrated using the fuzzy gamma operator to create the MPM. Accordingly, seven zones with high favorability were identified. Zones A, B, and C are recommended as high potential through field observation, laboratory studies, and Fuzzy logic integrating approach. The ICP-MS result indicated low grades of Cu and high grades of Pb, Zn, and Fe in carbonate, rhyolite, and tuff rocks as a sign of polymetallic mineralization in the FGBB. Results showed that altered intrusive rocks should receive the highest weight in the fuzzy geology layer. A combination of LSU and SAM methods could accomplish hydrothermal alteration mapping with high accuracy. PF analysis, when coupled with the intersection of faults and intrusive rocks, provides the necessary information to accurately produce a geological structure layer.

**Keywords** Mineral prospectivity map (MPM) · Photolineament factor (PF) · Stream sediment geochemistry · Fuzzy logic · Hydrothermal alteration · Ferdows–Gonabad–Bajestan belt (FGBB)

## Introduction

Mineral exploration requires a comprehensive approach to identify mineral indices, mainly in a large area. The existence of various conceptual models of mineral deposits, a variety of quantitative and qualitative data, and different expert opinions complicate the process of mineral prospectivity mapping and mineral exploration targeting (Yousefi et al., 2021). Mineral reserve mapping models are divided into three groups: knowledge-driven, data-driven, and hybrid methods (Carranza, 2017; Ghezelbash et al., 2021; Nykänen et al., 2008). Among the knowledge-driven techniques, the fuzzy logic method is often used due to the high impact of expert opinion on preparing the mineral prospectivity map (MPM) (Wambo et al., 2020; Yousefi & Carranza, 2017; Yousefi et al., 2013). Fuzzy logic is a scientific tool that has dynamically simulated a system possible without needing

---

✉ Mehdi Honarmand  
mehonarmand167@gmail.com

Zohreh Arjmand Lary  
arjmandzohreh7575@gmail.com

Hadi Shahriari  
shahriarihi@gmail.com

Mahdieh Hosseinjani Zadeh  
mh.hosseinjani@gmail.com

<sup>1</sup> Department of Ecology, Institute of Science and High Technology and Environmental Sciences, Graduate University of Advanced Technology, Kerman, Iran

<sup>2</sup> Department of Mining Engineering, Faculty of Engineering, Vali-e-Asr University of Rafsanjan, Rafsanjan, Iran

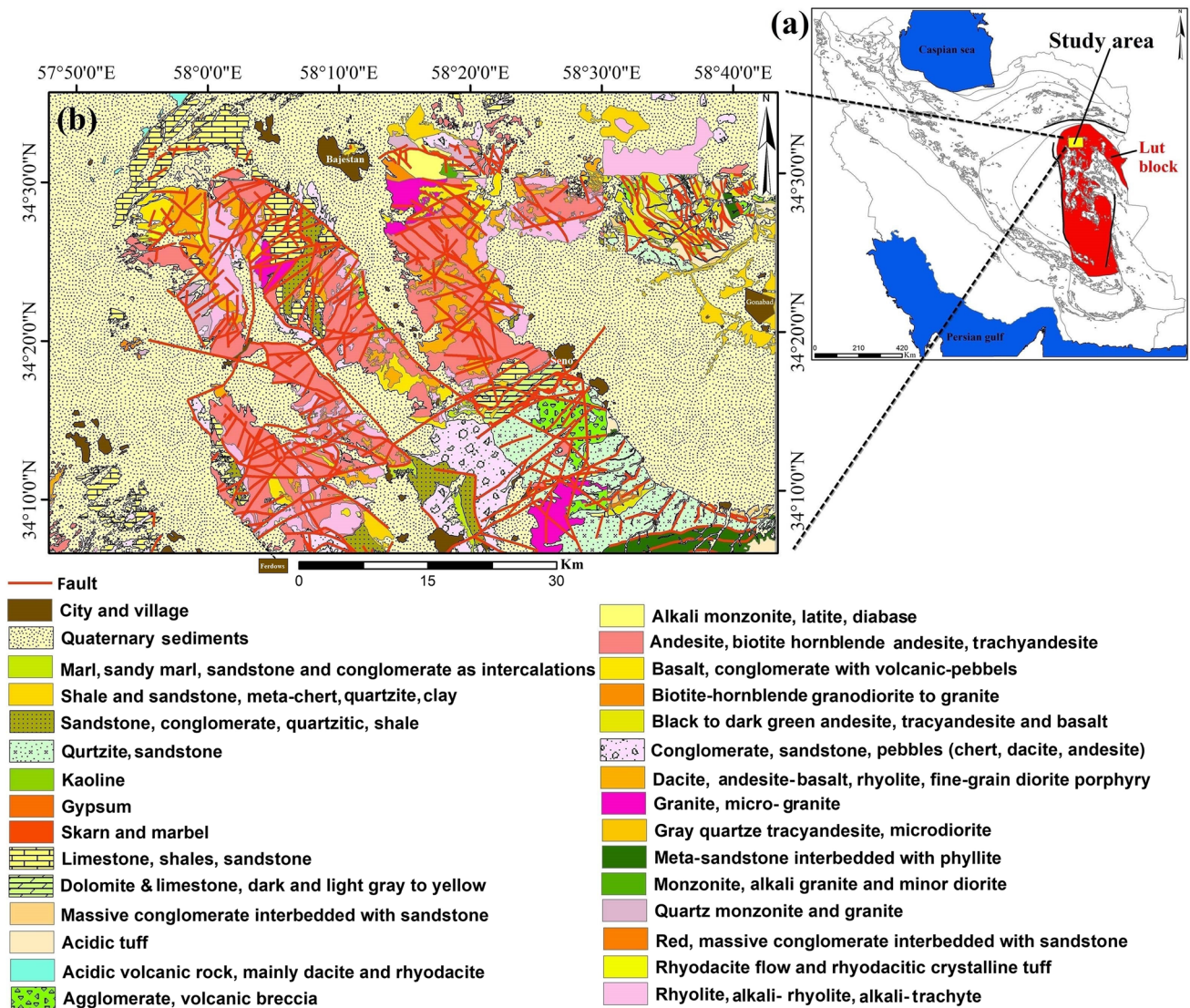


**Fig. 1** a Location of the study area along with the Lut block (Aghanabati, 2006), and b Geological map of the study area (Aghanabati, 2006)

detailed mathematical descriptions and using qualitative and quantitative data (Phillis & Andriantiatsaholoinaina, 2001).

Fuzzy logic has been successfully applied for integrating mineral exploration data to produce MPMs (e.g., Carranza, 2008, 2021; Carranza & Hale, 2001; Esmailoghli et al., 2021; Ford et al., 2016; Kashani et al., 2016; Pahlavani et al., 2020; Yousefi & Carranza, 2017; Yousefi et al., 2013). The high amount of input data leads to having more reliable results for making vital decisions in mineral exploration programs. Hence, geographic information system (GIS) platforms use various geo-datasets to establish a geo-database. At the regional scale, input data include geological maps, remote sensing data, geochemistry maps, and geophysical data (e.g., Carranza, 2008; Moradpour et al., 2021; Pahlavani et al., 2020).

Remote sensing technology has been widely employed in geological and mineral exploration by imaging different portions of the electromagnetic (EM) spectrum (e.g., Lyon & Lee, 1970; Goetz, 1983; Legg, 1994; Sabine, 1999; Roonwal, 2018). Thanks to worldwide coverage, spaceborne multispectral and hyperspectral sensors with different spatial resolutions are used for regional-scale mineral exploration through a very time- and cost-effective procedure (e.g., Mahanta & Maiti, 2018; Manuel et al., 2017). Advanced Spaceborne Thermal Emission and Reflection Radiometer (ASTER), Landsat TM/ETM +/OLI, and Sentinel with medium spatial resolution have been successfully performed to provide vital information about the geological structures, lithology, and alterations in recent years (Abrams & Yamaguchi, 2019; Adiri, 2020).

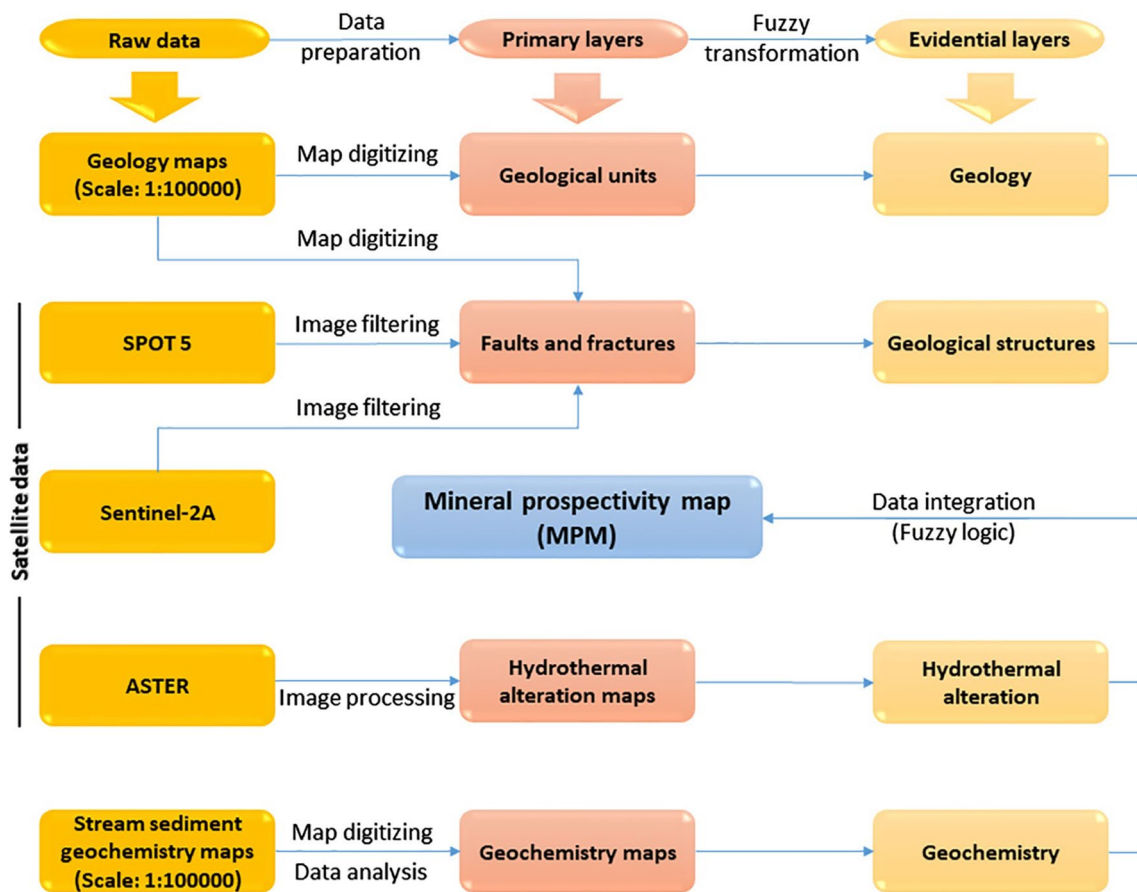


Fig. 2 Workflow of the research

Stream sediment geochemistry is an effective technique for finding clues of concealed mineral deposits in areas with well-developed stream drainage networks. The method has

been established to detect the composite products of an eroded and weathered probable ore body or its geochemical halos in downstream sediments (e.g., Behera & Panigrahi,

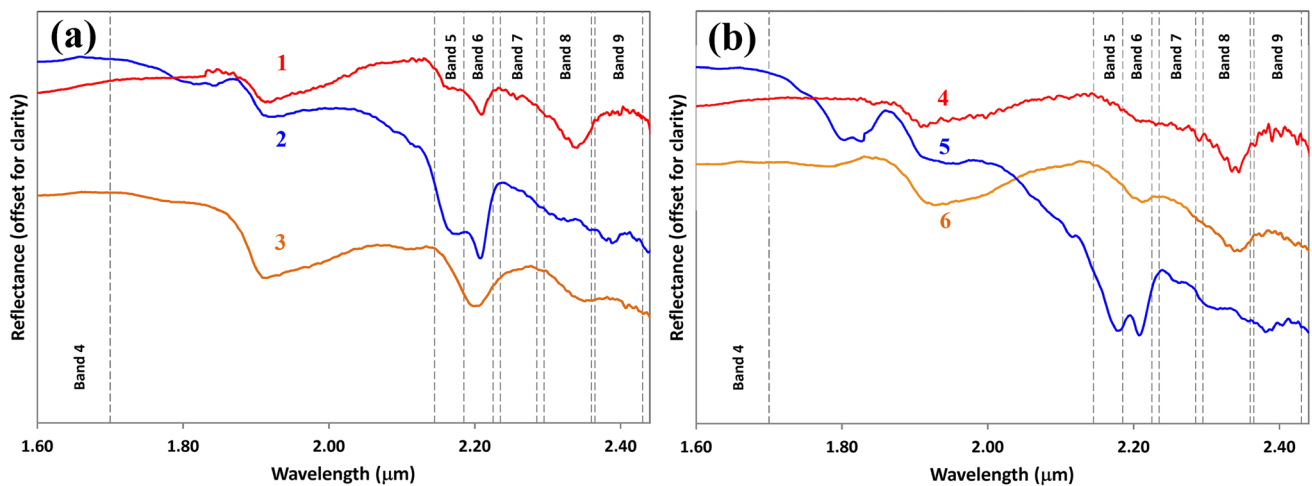


Fig. 3 Spectral reflectance curves of index minerals of hydrothermal alteration zones in the FGGB (ASTER bands are shown). (1) Muscovite and calcite, (2) Kaolinite, (3) Muscovite, (4) Calcite, (5) Kaolinite, and (6) Calcite and muscovite

2021; Sadeghi et al., 2015; Zuluaga et al., 2017). Based on the supposed deposit type, geochemical evidence layers are formed and integrated to create the mineral prospectivity map of the study area (Pahlavani et al., 2020; Yousefi et al., 2012, 2013). The stream sediment geochemistry maps have the appropriate extent for participating in data integration with other exploratory layers in the regional-scale investigation (e.g., Carranza & Hale, 1997; Ghasemzadeh et al., 2019; Saadati et al., 2020).

Ferdows–Gonabad–Bajestan belt (FGBB) situated in the south of Khorasan Razavi Province, Iran, is selected as the study area. This metallogenic belt was affected by volcanic activities in the Tertiary and Quaternary. The literature review indicated no systematic studies for prospecting mineral deposits. This research is performed to build the MPM of the FGBB. The fuzzy logic is used for integrating the exploratory geo-datasets. Geological maps, satellite data (ASTER, SPOT5, and Sentinel-2A), and stream sediment geochemistry maps are employed in the fuzzy logic method. The established MPM is validated through field and laboratory studies.

## Geological Settings

Lut block, with a length of 900 km, is located between the Nayband fault in the west and the Nehbandan fault in the east (Fig. 1a). This block is bounded by the Dorouneh fault in the north and the Jazmurian depression in the south, which is the forearc basin of the Makran subduction zone. Extensive volcanic activities of the Tertiary and Quaternary ages and recent earthquakes with faulting in Quaternary deposits are examples of the Lut block dynamics (Aghanabati, 2006). Mineralization in the Lut block has been suggested to be associated with either the intrusion of granite, diorite, or tertiary volcanic rocks. The northern Lut magmatic cycle has continued from the Late Cretaceous to the Late Oligocene. An assemblage of intrusive, semi-intrusive, and pyroclastic igneous rocks such as basaltic, andesitic, dacite, rhyolitic, tuff, and semi-deep lavas was created during the magmatism. Several mineral deposits and indices such as polymetallic deposits of copper, lead, zinc, antimony, mercury, and gold of vein and porphyry types have been reported in this region (Jung et al., 1983; Tarkian et al., 1983, 1984).

The study area was situated in the highlands of FGBB in the south of Khorasan Razavi Province and north of Lut

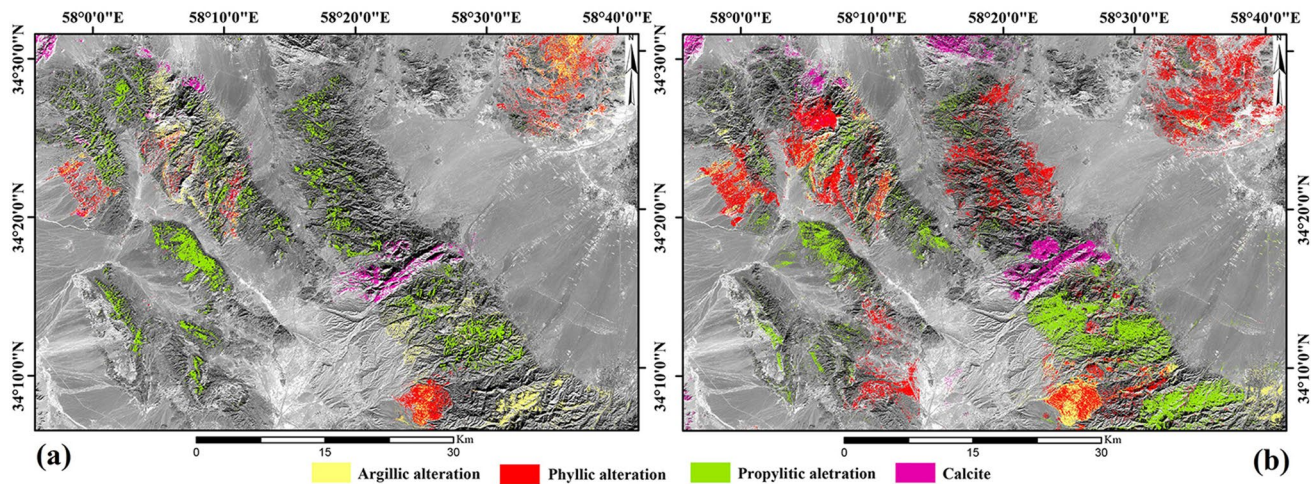


**Fig. 4** Hydrothermal alteration mapping by **a** LSU, and **b** SAM methods using ASTER SWIR bands

**Table 1** Accuracy assessment of LSU and SAM methods in mapping hydrothermal alterations

Alteration class	Phyllic	Argillic	Propylitic	Unaltered	Total	User Acc (%)
Phyllic	14	2	0	1	17	82.35
Argillic	1	11	0	1	13	84.62
Propylitic	0	1	16	3	20	80.00
Unaltered	3	0	3	21	27	77.78
Total	18	14	19	26	77	100
Prod. Acc (%)	77.78	78.57	84.21	80.77	100	80.33

block. The lithology includes igneous (mainly andesite, phyllite, and rhyolite), sedimentary (mainly limestone, dolomite, sandstone, and conglomerate), and metamorphic (quartzite) rocks (Fig. 1b).

## Data and Methods

In this research, three datasets including geological maps, satellite images, and stream sediment geochemistry data, provided information for creating the MPM (Fig. 2). Satellite data of ASTER (L1B product), SPOT5, and Sentinel-2A were analyzed using ENVI 5.3 software. The preprocessing procedure included crosstalk (only applied to ASTER shortwave infrared bands), atmospheric, and geometric corrections. Hydrothermal alterations were enhanced using the SAM and LSU methods. Geological structures like faults and fractures are considered as potential localities for mineralization. As a result, structural lineaments were extracted from high-resolution SPOT 5 and Sentinel-2A images and were analyzed using the photolineament factor (PF) analysis. Geological units and lineament features were extracted from geological maps in ArcGIS 10.3 software. Stream sediment

geochemistry data were analyzed using SPSS software version 21.0 to form the geochemistry evidence layer. Integrating the exploratory geo-datasets was performed in ArcGIS 10.3 software to build the MPM of the study area (Fig. 2). Fieldwork and laboratory studies were conducted to validate the results.

## Data

### Advanced Spaceborne Thermal Emission and Reflection Radiometer (ASTER) Data

ASTER is one of the five TERRA satellite sensors launched by NASA in 1999 (Abrams & Yamaguchi, 2019). It has a spatial resolution of 15, 30, and 90 m in the visible/near-infrared (VNIR), shortwave infrared (SWIR), and thermal infrared (TIR) bands, respectively. Six SWIR (2–3  $\mu\text{m}$ ) and five TIR bands (8–12  $\mu\text{m}$ ) provide suitable spectral resolution for mineral and geological mapping (e.g., Abrams & Yamaguchi, 2019; Wambo et al., 2020). ASTER SWIR bands were used in this research.

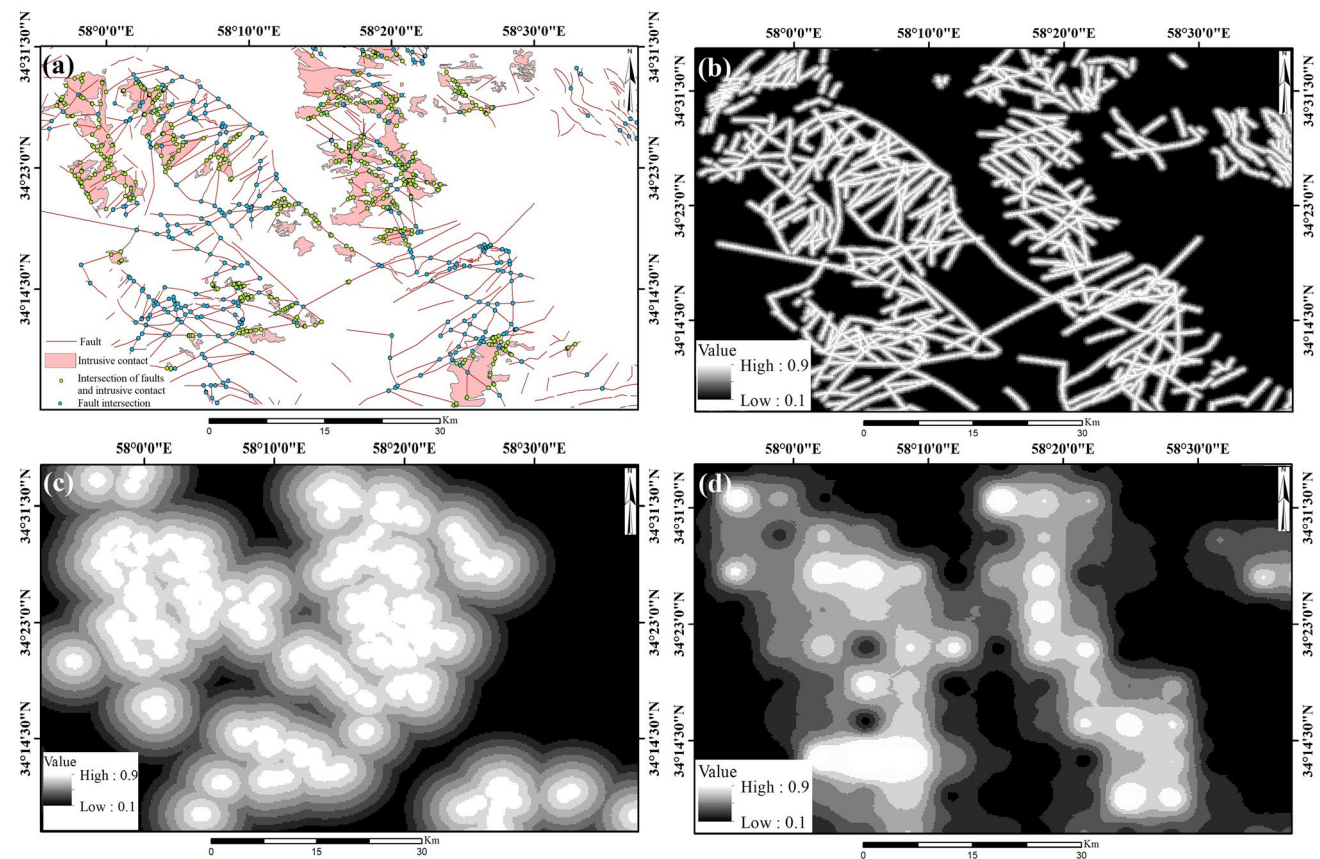


**Fig. 5** a Final map of the extracted faults in the study area, b Fuzzy map of proximity to faults, c Fuzzy map of intersection of faults and intrusive contacts, and d Fuzzy PF map of faults in the study area

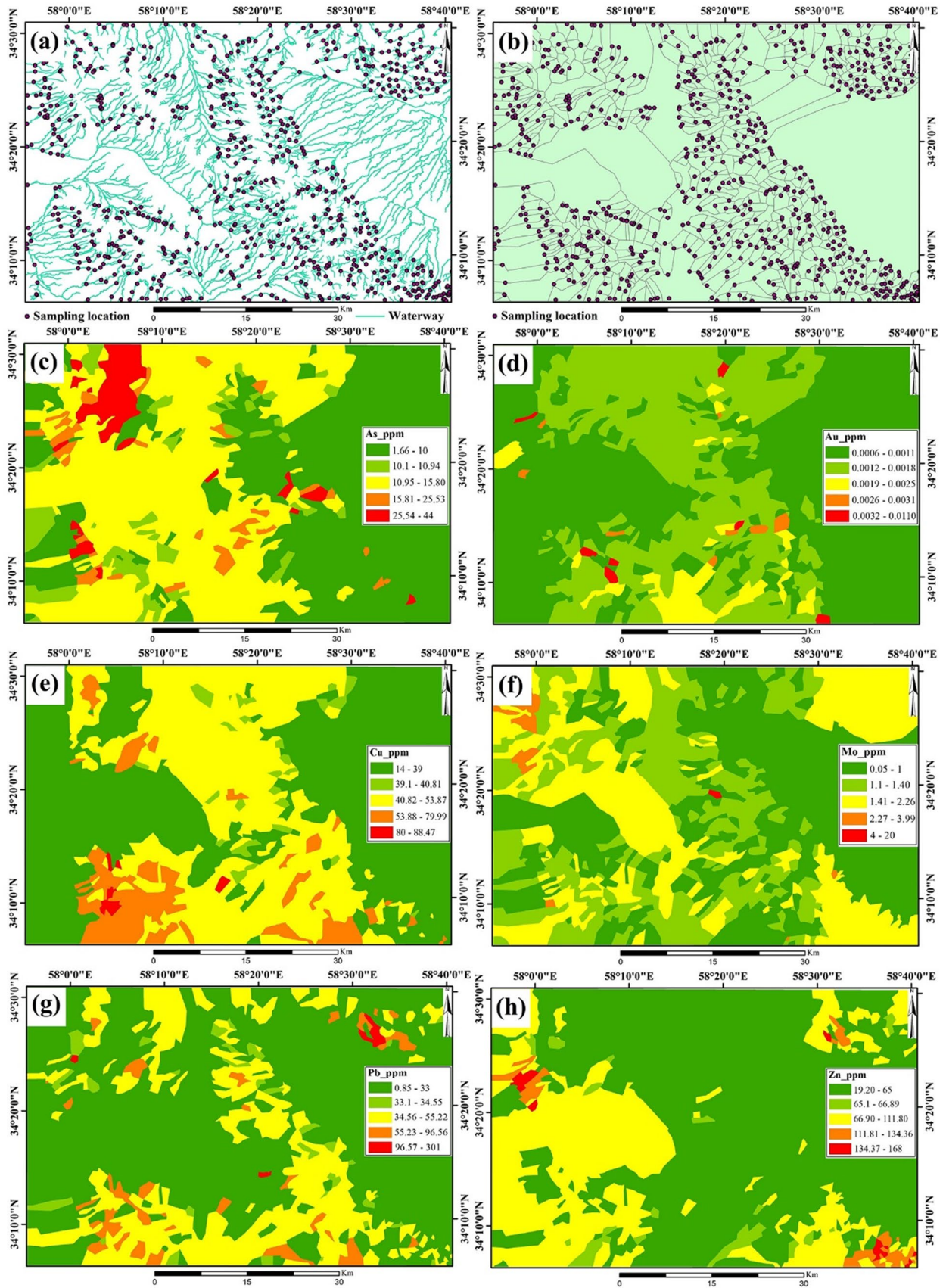


**Fig. 6** **a** Waterway network and the location of stream sediment samples, **b** Catchment basins and the location of stream sediment samples on waterways; stream sediment geochemistry maps of **c** As, **d** Au, **e** Cu, **f** Mo, **g** Pb, and **h** Zn in the FGGB

### Satellite Pour L'observation De La Terre 5 (SPOT5) Data

SPOT stands for satellite pour l'observation de la terre, meaning the earth observation satellite initiated by CNES in France and developed in collaboration with Belgium and Sweden. The last member of the SPOT series, i.e., SPOT 7, was launched into orbit in 2014; three of these satellites are currently imaging. SPOT 5 was launched on May 4, 2002, and can acquire images with the spatial resolution of 2.5, 5, and 10 m. It has three bands in the visible spectrum with a spatial resolution of 10 m, one SWIR band with a spatial resolution of 20 m, and one panchromatic band with a spatial resolution of 2.5 or 5 m (Toutin, 2004). Due to its high spatial resolution, its data were used to identify lineament features in the study area and perform the lithological mapping.

### Sentinel-2A Data

Sentinel-2 is a part of the Copernicus program designed and developed by the European Space Agency (ESA) to collect data from the earth's surface. The sentinel-2 mission comprises two imaging satellites, namely Sentinel-2A and Sentinel-2B. Sentinel-2A is currently in orbit and captures images with a spatial resolution of 10–60 m through 13 spectral bands in the visible, NIR, and SWIR spectral ranges (Drusch et al., 2012). The Sentinel-2A images are used for geological and structural mapping thanks to a variety of spectral bands.

### Geological Maps and Geochemical Data

Small-scale geological maps are generally available and provide helpful information for constructing a geodatabase in mineral exploration campaigns. Geological maps offer some primary data, such as geological units and regional structures. They are conventionally modified based on analyzing remote sensing data. In this research, geological maps (at the scale of 1:100,000) of Gonabad, Ferdows, Taherabad, Mahneh, Bajestan, and Qasemabad (Prepared by the Geological Survey of Iran-GSI) were used.

Many countries have undertaken regional stream sediment geochemical surveys to prepare base geochemistry maps for developing mineral exploration on a regional scale (Ranasinghe et al., 2008). Stream sediment geochemistry maps can offer a general scheme for the geochemical

distribution pattern of elements in the region. In Iran, GSI is responsible for preparing stream sediment geochemistry maps at the scale of 1:100,000 and smaller scales. Thus, stream sediment geochemistry maps of Gonabad, Ferdows, and Taherabad (at a scale of 1:100,000) were used to perform geochemical studies.

## Methods

### Spectral Properties of Hydrothermal Alteration Index Minerals

Hydrothermal alteration halo is one of the most important clues of possible mineralization. It is considered an exploratory target in mineral exploration campaigns. Some of the minerals of hydrothermal alteration zones exhibit spectral features that could be recognized by airborne/spaceborne remote sensing sensors (e.g.; Abrams & Yamaguchi, 2019; Adiri et al., 2020; Roonwal, 2018). Clay minerals (argillic alteration), sericite (phyllitic/sericitic alteration), and chlorite-epidote-calcite (propylitic alteration) present absorption/reflection features in the SWIR portion of the electromagnetic spectrum (Gupta, 2003). The clay minerals, sericite, chlorite, epidote, and calcite show high reflection in ASTER band 4. Illite and sericite/muscovite display an absorption feature at 2.20  $\mu\text{m}$  in ASTER band 6 due to the presence of Al–OH and another absorption with less intensity near 2.38  $\mu\text{m}$  in ASTER band 8 (Fig. 3) (Gupta, 2003; Hunt, 1977; Hunt & Ashley, 1979). Fe-oxyhydroxides minerals of phyllic and argillic zones, including jarosite, goethite, and hematite show spectral absorption near 0.44  $\mu\text{m}$  in the visible region. Electronic processes of the elements such as Cr, Mn,  $\text{Fe}^{3+}$ ,  $\text{Fe}^{2+}$ , and Ni in the crystal structure of these minerals cause spectral properties in the visible and NIR ranges (0.4–1.1  $\mu\text{m}$ ) (Fig. 3) (Hunt, 1977; Hunt & Ashley, 1979). In the argillic alteration zone, montmorillonite displays an absorption feature at 2.20  $\mu\text{m}$  due to the presence of Al–OH (Hunt, 1977; Hunt & Ashley, 1979). In addition, Al–OH causes two spectral features in the kaolinite spectrum. The first absorption feature is observed at 2.20  $\mu\text{m}$  in ASTER band 6 and the second absorption is found at 2.17  $\mu\text{m}$  in ASTER band 5 (Fig. 3). A mineral assemblage consisting of carbonates (calcite and dolomite), epidote, and chlorite in the propylitic alteration zone shows spectral absorption at 2.33–2.35  $\mu\text{m}$  in ASTER band 8 due to the molecular vibrations caused by Mg–OH, Fe, and  $\text{CO}_3$  (Fig. 3) (Hunt, 1977; Hunt & Ashley, 1979). Index minerals of silica alteration (mainly quartz), have minimum emission in ASTER bands 10 and 12 and maximum emission in ASTER bands 13 and 14 in the TIR range (Gupta, 2003; Hunt, 1977; Hunt & Ashley, 1979).

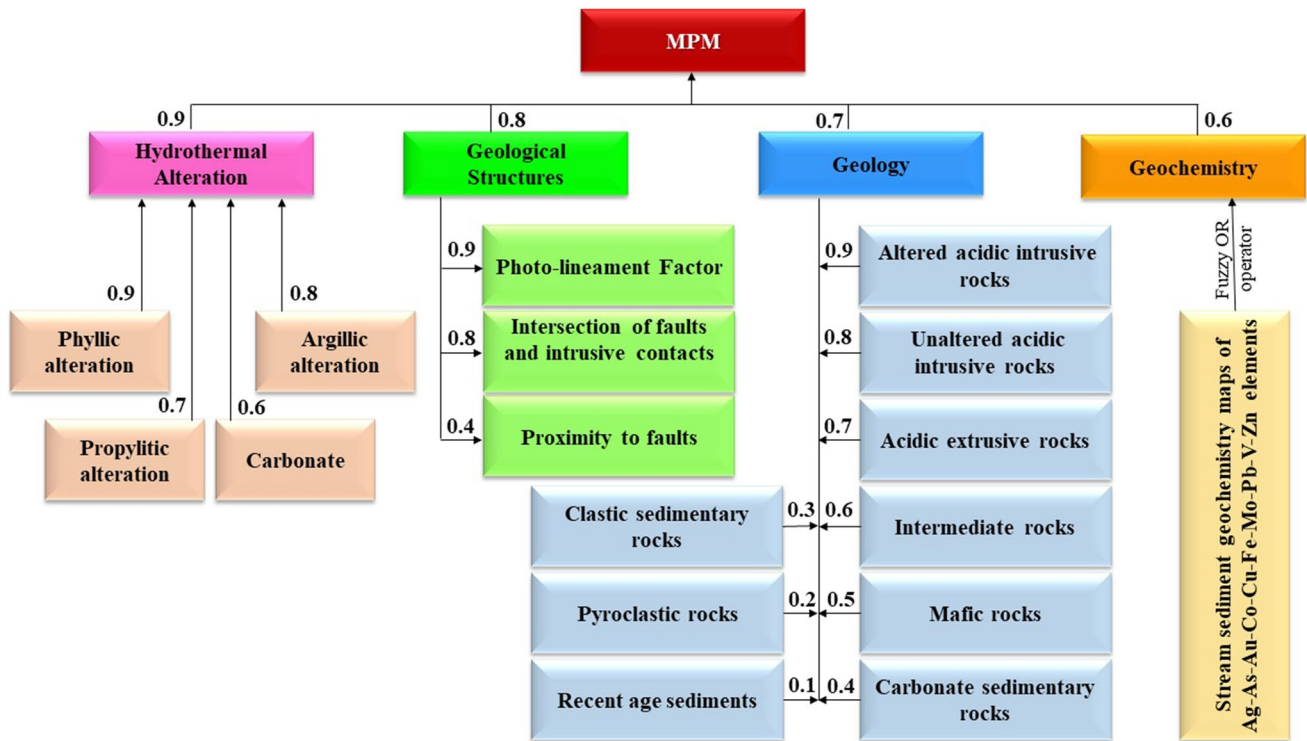


Fig. 7 The scheme for integrating data and assigned weights of layers to create the MPM in the study area

### Spectral Angle Mapper (SAM)

SAM is a supervised classification technique that maps the objects based on the degree of similarity between the image and reference spectra (Kruse et al., 1993). It calculates the angle between the reference and image spectra vectors in an  $n$ -dimensional ( $n$ -D) space. The smaller angle between these two vectors indicates more similarity. The user defines a threshold angle to classify the pixels based on the calculated angle (Kruse et al., 1993; Noori et al., 2019). Laboratory/field measurements, digital spectral libraries, or spectral profiling of the known points on the image are sources of preparing the reference spectrum. Typically, the image spectrum is employed to increase the result accuracy. Library spectra obtained from pure samples in the laboratory are inconsistent with the actual spectra due to impurities in the rocks.

### Linear Spectral Unmixing (LSU)

LSU determines the relative frequency of materials based on their spectral properties in multispectral images. The reflection of an image pixel is assumed to be the linear proportional combination of all the feature reflections at that pixel. The results of the spectral unmixing are in the form of a series of gray-scale images. Moreover, a root mean square (RMS) error image is generated. Brighter pixels indicate the higher frequencies and errors for the RMS error image. The results of this spectral technique depend on the input members, the variation of which changes the results. The LSU method has been successfully used for mineral mapping (Hubbard & Crowley, 2005; Sekandari, et al. 2020).

### Structural Data Analysis

Enhancing the geological structures is an essential part of remote sensing studies for mineral exploration applications. Structural analysis commonly includes intrusive contacts, fault density, fault intersections, and proximity to faults in mineral exploration targeting. Yousefi and Hronsky (2023) introduced a more efficient factor as the intersection of faults and intrusive contacts in preparing MPM. Such intersections



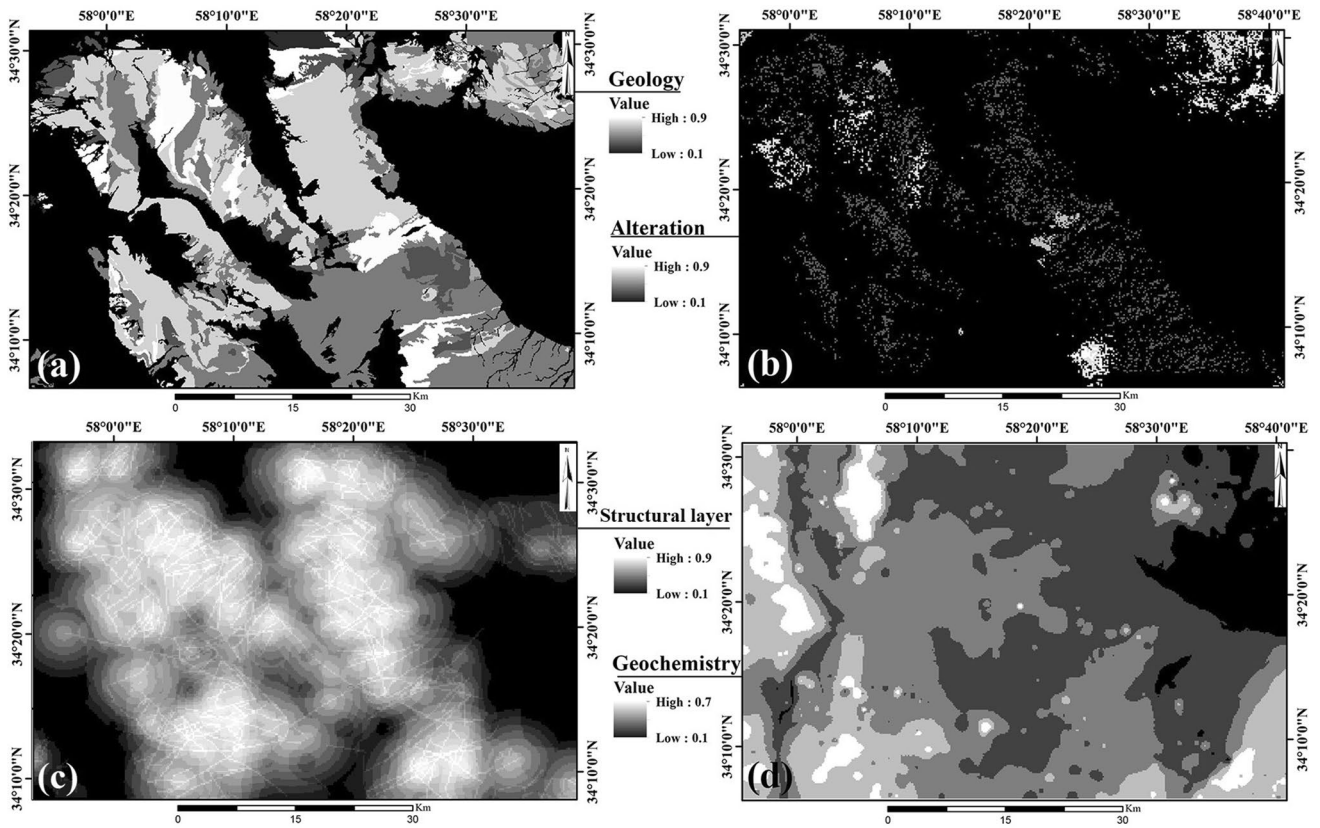


**Fig. 8** Fuzzy geo-datasets for data integration to establish the MPM in the FGGB: **a** geology layer, **b** alteration layer, **c** Geological structures layer, and **d** geochemistry layer

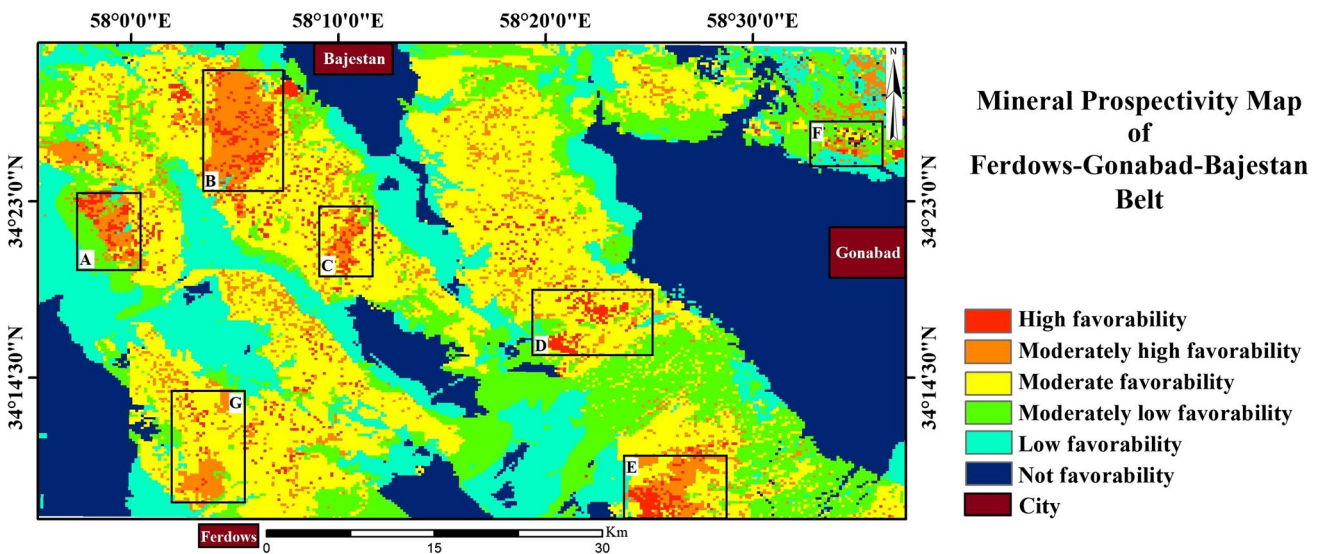


**Fig. 9** MPM of the FGGB and high potential localities for focusing mineral exploration activities

**Table 2** Chemical analysis of rock samples using the ICP-MS method

Zone	Element (ppm)								
	Ag	As	Co	Cu	Fe	Mo	Pb	V	Zn
A	7.80	50.00	3.00	788.40	18,560.00	38.10	14,540.00	4.30	38,820.00
A	39.10	33.50	1.30	782.50	20,320.00	6.40	51,690.00	10.40	41,610.00
B	0.40	709.00	1.00	8.00	2960.00	2.40	31.00	2.00	198.00
B	0.20	574.00	39.40	15.80	289,700.00	9.00	94.20	1004.00	1133.00
C	7.20	2.40	2.10	37.60	445.00	3.80	7467.00	3.60	586.00
C	0.70	11.00	17.70	2.40	42,740.00	3.20	1.50	9.00	194.00
D	4.00	33.00	5.30	1.00	17,658.00	6.60	322.00	36.00	52.00
D	0.20	8.00	3.70	18.00	25,194.00	0.60	13.00	2.00	38.00
E	0.10	2.50	16.30	3.30	51,780.00	5.10	10.50	9.60	121.00

can facilitate the passage of ore-forming metalliferous fluids and increase the efficiency of the ore mineralization procedure. In this study, three individual layers including the intersection of faults and intrusive contacts, the proximity of fault (by considering a buffer), and fault density (using photolineament factor) were employed to build the ultimate structural layer. Photolineament factor (PF) is a function of the number, length, and intersection of lineaments (e.g., faults). That is usually applied for analyzing lineaments in remote sensing studies for mineral exploration objectives. To calculate the PF, a rectangular network is used. PF is calculated for each network cell according to Eq. 1 (Hardcastle, 1995; Hardcastle et al., 1997):

$$PF = \frac{a}{A} + \frac{b}{B} + \frac{c}{C} \quad (1)$$

where 'a' is the number of faults per cell, 'A' is the mean number of faults in the whole network, 'b' is the fault length per cell, 'B' is the mean length of all the faults, 'c' is the number of fault intersections per cell, and 'C' is the mean fault intersection in all cells with fault intersections. PF values are calculated for the center of each cell and, then, interpolated by the inverse distance weighting (IDW) method.

Directional filters at 45 and 90 degrees and the Sobel filter were employed to detect lineaments with specific trends in Sentinel-2A and SPOT 5. After plotting the faults, ArcGIS software was performed to draw a rectangular network with the dimension of 5000 m × 5000 m. For each cell, the number and length of faults, as well as the number of fault intersections, were determined for calculating the PF. The geological structures layer was created from the results of PF analysis.

### Geological and Geochemical Data Analysis

Geological maps of Gonabad, Ferdows, Taherabad, Mahneh, Bajestan, and Qasemabad were digitized to extract geological units and regional faults. The regional faults

were used in structural analysis. Stream sediment geochemistry data was derived by digitizing Gonabad, Ferdows, Taherabad, Mahneh, Bajestan, and Qasemabad geochemistry maps. Discrimination of geochemical anomalies related to ore mineralization from the background is a challenging task (Carranza & Hale, 1997; Ghasemzadeh et al., 2019). This challenge has encouraged researchers to improve approaches for defining the best threshold value. These approaches are classified into frequency-based and spatial frequency-based techniques (e.g., Chiprés et al., 2009; Ghasemzadeh et al., 2019; Yang et al., 2015). Ore-forming processes control the spatial distribution of elements and minerals that must be understood through geochemical exploration campaigns (Esmailoghli et al., 2021). Multivariate analysis can help specify the multi-element anomalous signature of mineral deposits (Yousefi et al., 2012). Factor analysis has been successfully used for multivariate analysis of stream sediment geochemical data (e.g., Borovec, 1996; Helvoort et al., 2005; Reimann et al., 2002; Yousefi et al., 2012, 2014). This method can determine the inherent variability in stream sediment data using a set of elements depending on the mineral deposit-type sought (Yousefi et al., 2012). In this research, factor analysis was used for discriminating anomalous areas for Au, Ag, As, Co, Cu, Fe, Mo, Pb, V, and Zn elements.

### Fuzzy Logic

Fuzzy logic can express the degree of certainty or accuracy of a statement by a number between 0 and 1 where a value of 0 represents full non-membership and a value of 1 represents full membership. Experts assign a fuzzy membership (Fuzzy score) between 0 and 1 to any evidential layer based on the supposed ore deposit. After assigning fuzzy scores, PMP is built using fuzzy logical operators such as AND, OR, NOT, and gamma (Bonham-Carter, 1994; Carranza & Hale, 2001). In this study, the OR operator was used to combine geochemical maps of Au, Ag,

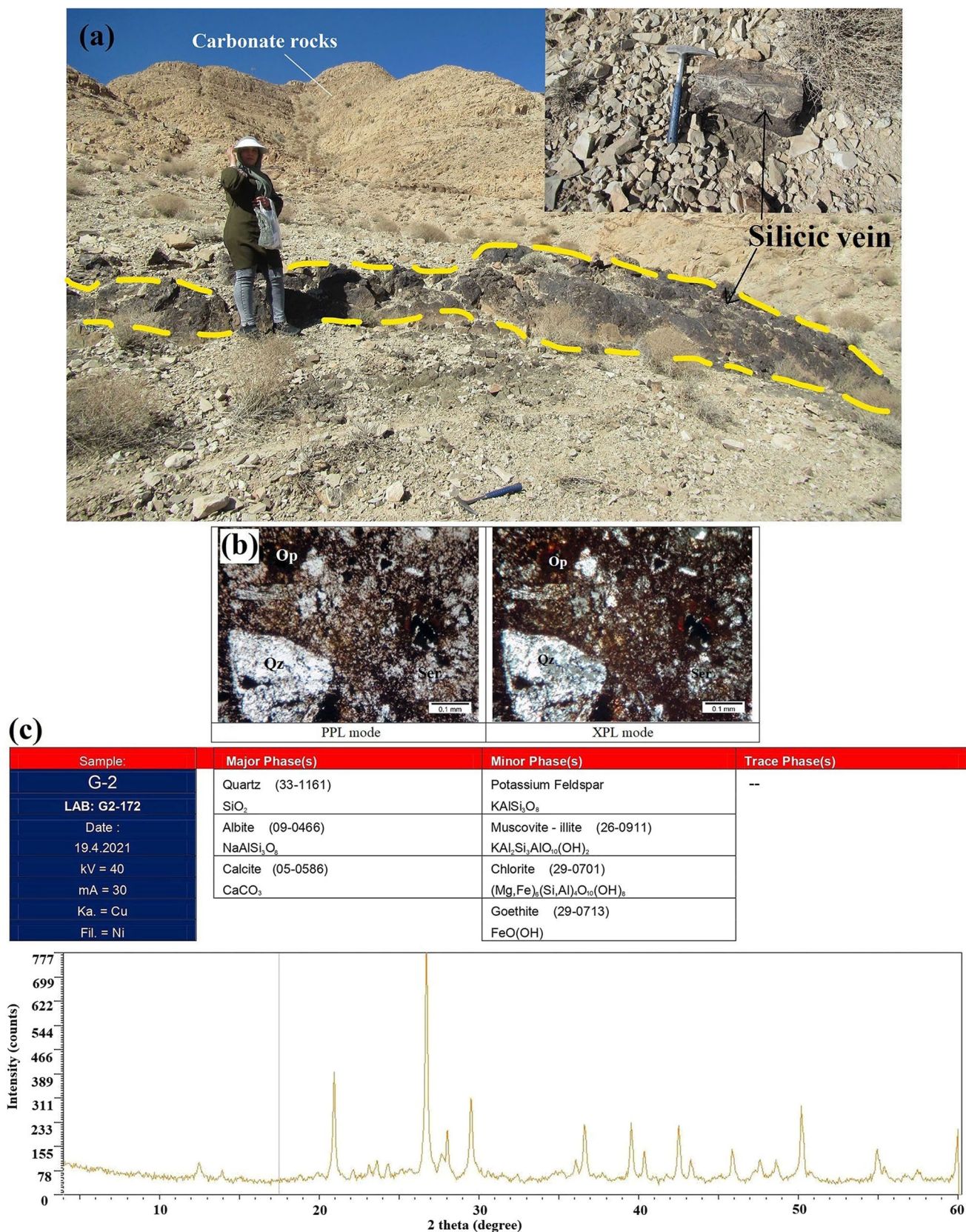
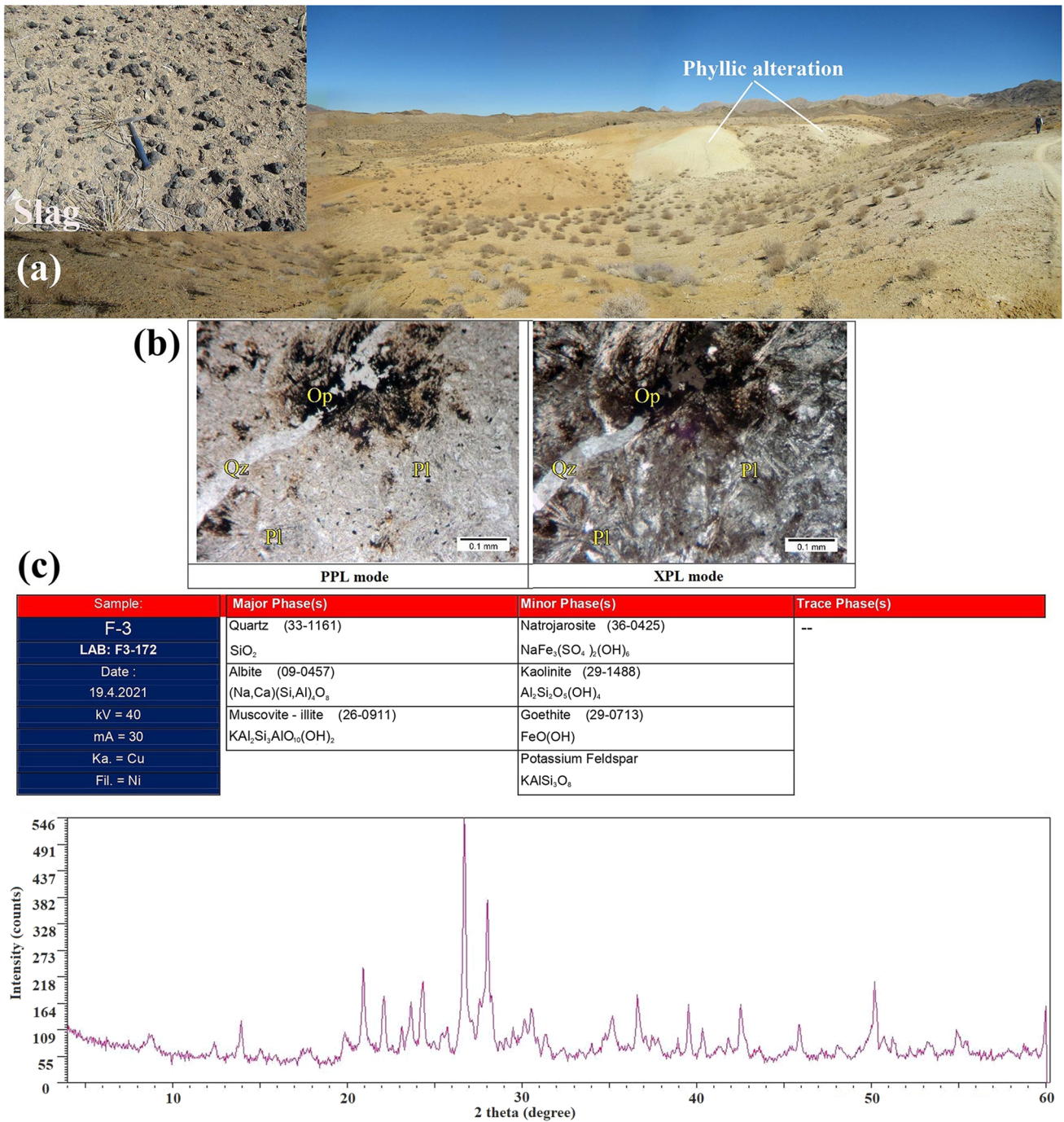


Fig. 10 a Silicic vein in zone A, b Thin section of a lithic tuff shows sericite (Ser), opaque (Op), and quartz (Qz) minerals, c Result of XRD analysis



**Fig. 11** a General view of zone B along with an image of the slags found in zone B, b Thin section of a basalt contains plagioclase (Pl), opaque (Op), and quartz (Qz) minerals, c Result of XRD analysis

As, Co, Cu, Fe, Mo, Pb, V, and Zn elements. The gamma operator was performed to integrate all the evidential layers for establishing the MPM of the study area.

### Fieldwork and Laboratory Studies

Field investigation and laboratory studies were conducted for anomaly checking and result validation. Fieldwork included taking photos, GPS readings, and rock sampling. Rock samples were utilized for spectroscopy study using a FieldSpec3<sup>®</sup> spectroradiometer. As a result, a spectral

library was formed to be used in the image processing stage. A petrographic study was performed by thin section and XRD analysis. Rock samples of anomalous areas were analyzed using the ICP-MS method.

## Results and Discussion

### Hydrothermal Alteration Layer

Outcrops of volcanic rocks are seen with the northwest-southeast strike. These rocks are affected by various types of hydrothermal alteration. Determining the types of hydrothermal alteration is essential to assign an appropriate fuzzy score for creating the hydrothermal alteration layer. Phyllic and argillic alterations usually have a higher potential of hosting metallic mineralization.

Figure 3a shows the results of image classification of ASTER SWIR bands using the LSU method. The propylitic alteration zone was enhanced by epidote and chlorite mineral spectra. Volcanic, andesitic, and rhyolitic units are usually affected by propylitic alteration in the region (Figs. 1 and 4a). Comparing Figs. 1 and 4a indicates that the phyllic alteration zone covers granitic, microgranitic, quartz monzonitic, rhyolitic, andesitic, dacitic, and trachyandesitic lithologies. Argillic alteration is observed in granitic, microgranitic, quartz monzonitic, rhyolitic, acidic tuff, and trachyandesitic units (Figs. 1 and 4a).

Figure 3b shows the hydrothermal alterations detected by the SAM method in the study area. Laboratory spectra taken from the rock samples were used as the reference spectra. The yellow parts represent argillic and phyllic alterations, which were found in granitic, dacitic-andesitic, quartz monzonitic, and trachyandesitic units. Propylitic alteration was observed in the areas with andesitic lithology (Figs. 1 and 4b).

Hydrothermal alteration zones presented in Fig. 4 were verified through fieldwork and laboratory studies. The result showed that the LSU method enhanced phyllic, argillic, and propylitic alterations more accurately than the SAM method. SAM method specified carbonate units more accurately, especially in the north of the study area (Fig. 4b). Thus, phyllic, argillic, and propylitic alteration classes obtained from the LSU method and a class containing carbonate occurrences enhanced by the SAM method were selected to create the hydrothermal alteration layer. Table 1 shows the accuracy assessment of hydrothermal alteration mapping by LSU and SAM methods.

### Geological Structures Layer

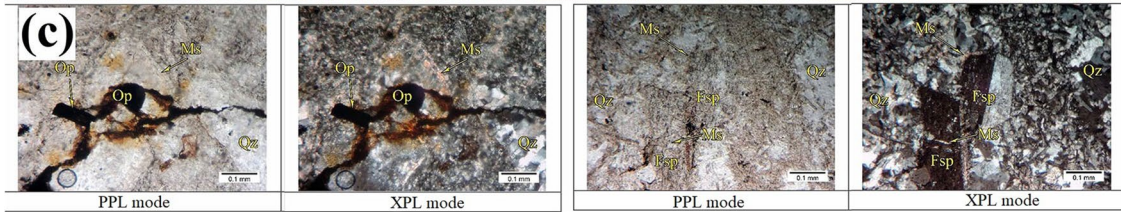
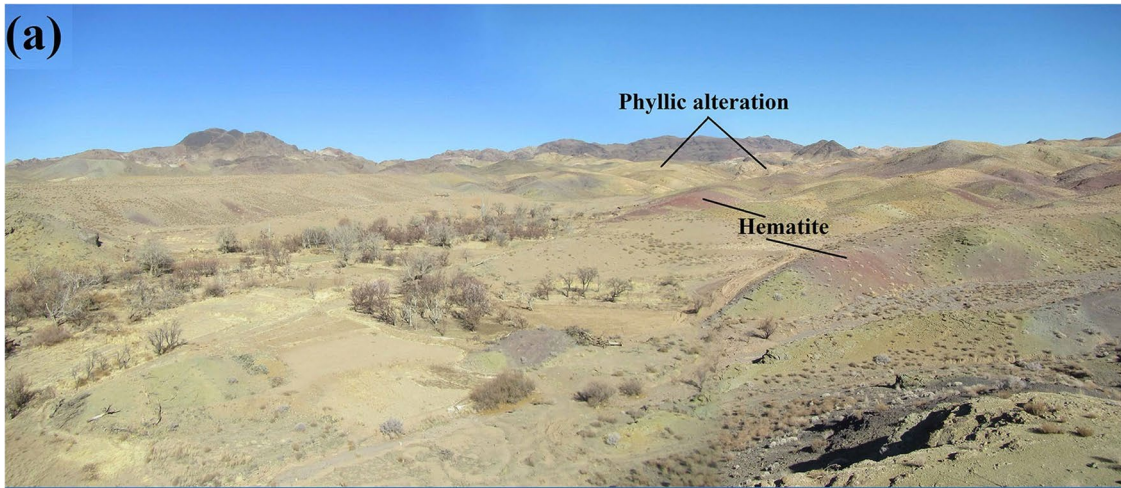
Faults and fractures are considered suitable channels for circulating hydrothermal solutions, resulting in the dissolution

of elements and their redistribution in the form of various minerals in the earth's crust. Studying hydrothermal alterations and their relationship with faults is of great importance to specify zones with high potential for metallic mineralization. Sentinel-2A and SPOT5 images were used to extract the structural lineaments using two-directional filters at 45 and 90 degrees and one non-directional Sobel filter. Accordingly, most of the faults had the northwest-southeast strike in the study area (Fig. 5a). The intersection of faults and the intersection of faults and intrusive contacts are presented in Fig. 5a. Faults can affect the adjacent area by injecting fluid flux through lateral fractures. The proximal area around the faults, thus, was attended by considering a buffer in the study area (Fig. 5b). The faults, the intersection of faults, and the intersection of faults and intrusive contacts define high-permeability areas for directing fluid flux. Figure 5c shows the Fuzzy map of the intersection of faults and intrusive contacts in the FGGB. In order to emphasize the density of faults in the study area, the PF map was built using the number, length, and intersections of faults. The PF map created by interpolating PF values using the IDW method shows the areas with the highest rate of fault density in the light color in Fig. 5d.

### Geology and Geochemistry Layers

FGGB is a far and rugged terrain that caused it to remain geologically unknown. No major metallic mine is in work and mining activities are limited to the excavation of some non-metallic mines. Volcanic activities in FGGB occurred in the Tertiary and Quaternary. Intrusive bodies usually have experienced a degree of hydrothermal alteration in the study area. To reconstruct the evidential geology layer, it is essential to define the appropriate weight for each geological unit. The highest weight was assigned to altered intrusive rocks that have a higher potential for hosting metallic mineralization. Unaltered intrusive and volcanic rocks received high to medium weights. Some carbonate units were enhanced using ASTER images in the study area (Fig. 4b). The proximity of volcanic rocks to carbonate rocks may have contributed to Zn–Pb mineralization in the study area. Thus, a medium weight was assigned to carbonate rocks. Low weights were assigned to sedimentary rocks.

ArcGIS software was used for digitizing stream sediment geochemistry maps. Catchment basins and waterway network of the study area were created (Figs. 6a and b). The background, threshold value, and anomaly were separately determined for Au, Ag, As, Co, Cu, Fe, Mo, Pb, V, and Zn elements. Some of the geochemistry maps are provided in Fig. 6. High values of Fe, Pb, and Zn were detected, while Cu, Co, and Au presented low values. ArcGIS software helped to compare geochemistry results with



Sample:	Major Phase(s)	Minor Phase(s)	Trace Phase(s)
E-2	Quartz (33-1161)	Muscovite - illite (26-0911)	Hematite (33-0664)
LAB: E-2	SiO <sub>2</sub>	KAl <sub>2</sub> Si <sub>4</sub> AlO <sub>10</sub> (OH) <sub>2</sub>	Fe <sub>2</sub> O <sub>3</sub>
Date:	Albite (09-0466)	Potassium Feldspar	
19.4.2021	NaAlSi <sub>3</sub> O <sub>8</sub>	KAlSi <sub>3</sub> O <sub>8</sub>	
kV = 40			
mA = 30			
Ka. = Cu			
Fil. = Ni			

(d)

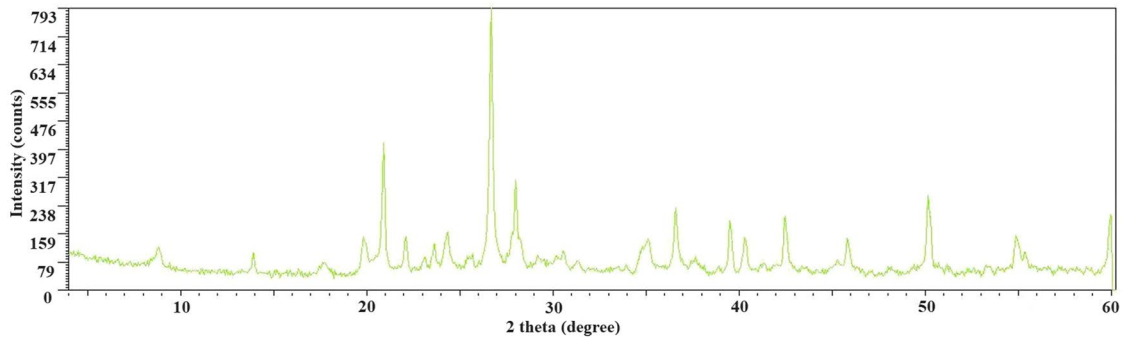


**Fig. 12** **a** General view of zone C, **b** Outcrop of an immature gossan, **c** Thin sections of rhyolite shows muscovite (Ms), quartz (Qz), feldspar (Fsp), and opaque (Op) minerals, **d** Result of XRD analysis

geology to interpret the geochemical distribution pattern of elements. The highest anomalies of Au were found in dacitic, andesitic, and rhyolitic units, not associated with the hydrothermal alterations in the study area (Figs. 1b and 6d). Ag anomalies were identified in the altered andesitic and dacitic units, and anomalous values of Ag were obtained from the chemical analysis of rock samples. Ag anomalies were related to argillic and phyllic alterations. Anomalies of As were found in carbonate-shale, sandstone, granitic, and microgranitic units (Figs. 1b and 6c). The rock samples also showed As anomalies. Co anomalies were observed in unaltered carbonate, shale, and limestone units and quartz monzonitic unit, which was associated with phyllic, argillic, and to some extent, propylitic alterations. Cu had the highest anomalies in andesitic, dacitic, and trachyandesitic units, which were not associated with alterations in the study area (Figs. 1b and 6e). Moreover, the rock samples taken from quartz monzonitic units showed the highest content of Cu, which was related to phyllic and argillic alterations. Fe anomalies were observed in hydrothermally altered andesitic and rhyolitic units. The rock samples also displayed Fe anomalies. The highest anomalies of Mo were identified in unaltered andesitic units (Figs. 1b and 6f). The rock samples taken from quartz monzonitic units showed Mo anomalies, associated with propylitic alteration. Pb anomalies were found in quartzite and sandstone units (Figs. 1b and 6g). However, the rock samples with Pb anomalies were identified in sandstone, carbonate, and quartz monzonitic units. V anomalies were observed in limestone, shale, sandstone, and granitic units, which were associated with propylitic and argillic alterations. The rock samples taken from these areas also showed V anomalies. Zn anomalies were found in quartz monzonitic and carbonate units, and the rock samples taken showed Zn anomalies (Figs. 1b and 6h).

### Data Integration

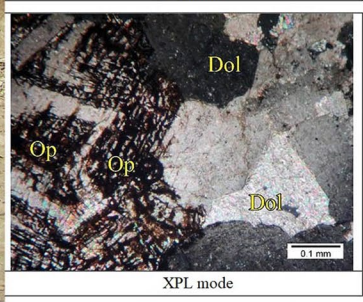
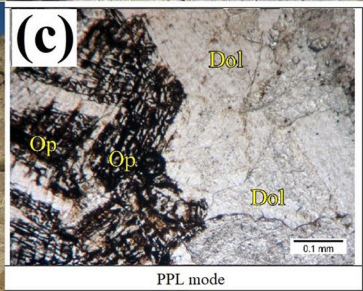
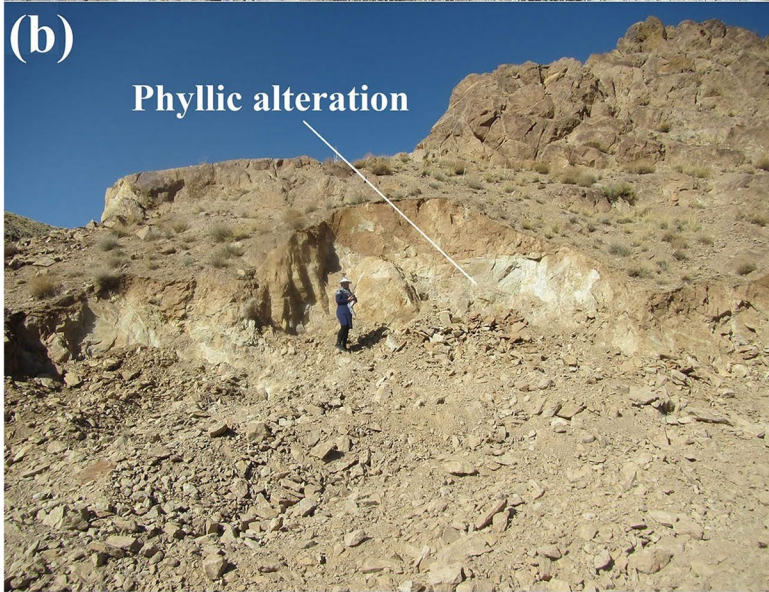
Figure 6 shows the scheme for integrating data using the fuzzy logic method. Evidential layers and assigned weights were defined based on the knowledge of experts. The geological map of the study area was one of the main input layers. Based on Fig. 6, geological units were categorized into nine classes, including altered acidic intrusive bodies, unaltered acidic intrusive bodies, acidic extrusive bodies, intermediate bodies, mafic bodies, carbonate sedimentary rocks, clastic sedimentary rocks, pyroclastic rocks, and the recent age sediments. Each class received a value from 0.9 to 0.1 by the fuzzy method (Figs. 7 and 8a).

The final hydrothermal alteration map was established based on the results of LSU and SAM methods. Argillic, phyllic, and propylitic alteration were derived as the outputs of the LSU method, and carbonate units were selected based on the SAM results (Fig. 3). Considering the region's geology and geochemical anomalies, mineralization was more likely associated with phyllic and argillic alterations. According to the importance of alterations and their relationship with the type of mineralization, phyllic, argillic, propylitic, and carbonate zones were assigned the values of 0.9, 0.8, 0.7, and 0.6, respectively (Figs. 7 and 8b). Due to the importance of faults in the formation of mineral deposits, the evidential layer of geological structures was produced (Fig. 8c). Figure 8c was built by integrating three layers including the proximity to the fault (Fig. 5b), the intersection of faults and intrusive contacts (Fig. 5c), and PF maps (Fig. 5d). Since the fault numbers, fault lengths, and fault intersections are taken into account, PF analysis can be representative. The map of the intersection of faults and intrusive contacts is also crucial for producing the evidential layer of geological structures due to conducting ore-forming fluids. Stream sediment geochemistry maps of Au, Ag, As, Co, Cu, Fe, Mo, Pb, V, and Zn elements were integrated by the fuzzy OR operator. Figure 8d shows the fuzzy geochemistry map of the study area, which was classified into seven levels from 0.1 to 0.7.

The geology layer was assigned with the highest weight (Fig. 7). Altered intrusive bodies were more valuable member due to their hydrothermal alteration and high geochemical anomalies compared to the other geological units. The hydrothermal alteration layer was specified with a weight of 0.8 based on expert opinion. Phyllic and argillic zones are appropriate places for the exploration of metallic mineralization. The geological structures and geochemistry layers received fuzzy scores of 0.7 and 0.6, respectively. Finally, evidential layers including geology, alteration, geological structures, and geochemistry were integrated by the fuzzy gamma operator ( $\gamma = 0.95$ ) to establish the MPM of the study area (Fig. 9).

### Fieldwork and anomaly checking

Based on Fig. 9, seven areas with the highest favorability were identified. Field investigation and rock sampling were undertaken in the A, B, C, D, E, and F zones. Zone G was left for future study due to time constraints. About 120 rock samples were spectrally studied using the FieldSpec3@ spectroradiometer to validate the results of image processing. More than 110 rock samples were analyzed using the ICP-MS method. Some results are provided in Table 2. The chemical analysis of rock samples was used to check the results of data integration in six mineral potential zones.



Sample:	Major Phase(s)	Major Phase(s)	Minor Phase(s)
A-Z	Quartz (33-1161)	Dolomite (36-0426)	Goethite (29-0713)
LAB: AZ-172	SiO <sub>2</sub>	CaMg(CO <sub>3</sub> ) <sub>2</sub>	FeO(OH)
Date :	Calcite (05-0586)	Chlorite (29-0701)	
19.4.2021	CaCO <sub>3</sub>	(Mg,Fe) <sub>3</sub> (Si,Al) <sub>2</sub> O <sub>10</sub> (OH) <sub>2</sub>	
kV = 40	Albite (09-0466)		
mA = 30	NaAlSi <sub>3</sub> O <sub>8</sub>		
Ka = Cu	Muscovite - illite (26-0911)		
Fil. = Ni	KAl <sub>3</sub> Si <sub>3</sub> AlO <sub>10</sub> (OH) <sub>2</sub>		

(d)

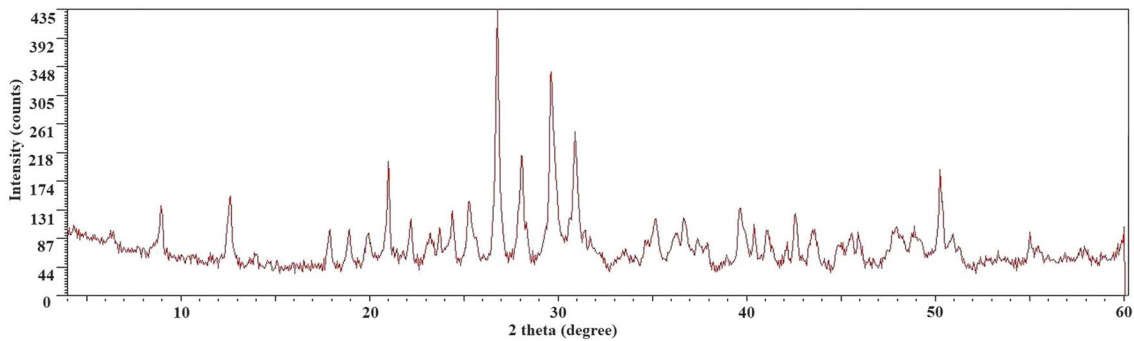




**Fig. 13** **a** An outcrop of a dolomitic carbonate unit in zone D, **b** Outcrop of phyllic alteration and carbonate rock in zone E, **c** Thin section shows dolomite (Dol) and opaque (Op) minerals, **d** Result of XRD analysis

Zone A mainly includes quartz monzonitic and lithic tuff units with phyllic and argillic alterations. Propylitic alteration covers a small area. Figure 10a displays an outcrop of a silica vein in adjacency to phyllic alteration. A thin section of a lithic tuff is seen in Fig. 10b which shows muscovite and opaque inside quartz, feldspar, and plagioclase. Muscovite, calcite, chlorite, and goethite were reported in the XRD analysis (Fig. 10c). Figure 3 presents the effect of muscovite (absorption feature in ASTER band 6) and chlorite/calcite (absorption feature in ASTER band 8) on the spectral reflectance curve no. 1.

Andesite and sandstone were the principal rock types of zone B. As shown in Fig. 11a, phyllic is the dominant alteration type. Old slags were seen in zone B as good evidence of mineralization (Fig. 11a). Figure 11b exhibits a thin section of basalt that shows opaque minerals and silica veins. Based on the XRD result, muscovite was in the major phase, while kaolinite and goethite were in the minor phase (Fig. 11c). In Fig. 3, kaolinite causes a shoulder in the ASTER band 5 on the spectral reflectance curve no. 2. Fe grade was 33,706–45,300 ppm (Table 2).

Zone C was specified by rhyolitic lithology with phyllic and argillic alterations. Figure 12a exhibits the general view of zone C which indicates the intensity of hydrothermal alteration. Figure 12b shows an immature gossan in zone C as a sign of intense chemical leaching. Figure 12c presents muscovite, clay minerals, opaque, and silica veins in the rhyolite thin section. Figure 3 shows a sharp absorption feature in the ASTER band 6 on the spectral reflectance curve no. 3 due to the presence of muscovite. Figure 12d displays the XRD result of a sample in zone C that contains muscovite in the minor phase.

Zone D is marked by a carbonate unit with severe propylitic alteration for volcanic rocks. Figure 13a presents an outcrop of carbonate rocks in zone D. Spectral reflectance curve no. 4 in Fig. 3 illustrates the calcite spectrum (absorption feature in ASTER band 8) belonging to a sample obtained from zone D.

Zone E represents granitic lithology with severe phyllic and argillic alterations. Figure 13b shows phyllic alteration in adjacency to carbonate rocks. In the thin section, dolomite and opaque minerals were observed (Fig. 13c). The XRD analysis showed muscovite and calcite in the major phase and dolomite in the minor phase (Fig. 13d). The effects of muscovite (absorption feature in ASTER band 6) and calcite (absorption feature in ASTER band 8) were apparent on the spectral reflectance curve no. 5 in Fig. 3.

Zone F shows andesitic, trachyandesitic, and basaltic lithologies with phyllic, argillic, and partially propylitic alterations. Figure 14a displays a kaolinite mine in zone F. In the thin section of Fig. 14b, quartz and opaque minerals are observed. Kaolinite and quartz form a major phase based on the XRD result (Fig. 14c). The spectral reflectance curve no. 6 in Fig. 3 exhibits absorption features of kaolinite as absorption in ASTER band 6 and a shoulder in ASTER band 5.

## Conclusion

The FGGB is one of the unknown metallogenic belts in Iran that presents surficial clues of metallic mineralization (e.g., extensive hydrothermal alteration, gossans, and old slags). Volcanic activities in the Tertiary and Quaternary have developed hydrothermal alteration in intrusive bodies and surrounding volcanic and volcano-sedimentary rocks. Faults and fractures have had a vital role in distributing hydrothermal solution and mineralization. In this research, the MPM of the FGGB was proposed by integrating various geo-datasets. The geology layer is a base geo-dataset for constructing the MPM. The importance of the geology layer resulted in defining two criteria including rock type and alteration for assigning proper weights. Altered and unaltered intrusive bodies should have the highest weights in the geology layer, while sedimentary rocks were specified with lower weights. Carbonate rocks, because of the potential of hosting Pb–Zn deposits, were assigned with moderate weights. Carbonates and well-known hydrothermal alterations (e.g., phyllic, argillic, and propylitic alterations) exhibit specific spectral features in the SWIR region of the EM spectrum that can be enhanced using ASTER data. Thus, ASTER SWIR bands were utilized to specify hydrothermal alterations. The application of both LSU and SAM methods resulted in deriving adequate information about typical alterations in the study area. It is recommended to perform LSU and SAM methods to get reliable results in areas with similar geological settings. Phyllic, argillic, and propylitic alterations were specified in the study area and the results were verified through field and laboratory studies. Phyllic and argillic alterations were often matched with intrusive bodies in the study area. As a result, they were specified with high weights in the hydrothermal alteration layer. The geological structures layer contributed to data integration to emphasize the importance of faults and fractures in hydrothermal mineralization. Regional faults and fractures can be extracted from small-scale geological maps, but in detail, satellite data provide helpful information about the geological structures. Thanks to worldwide coverage and high-resolution data, Sentinel-2 and SPOT 5 can be utilized for mapping

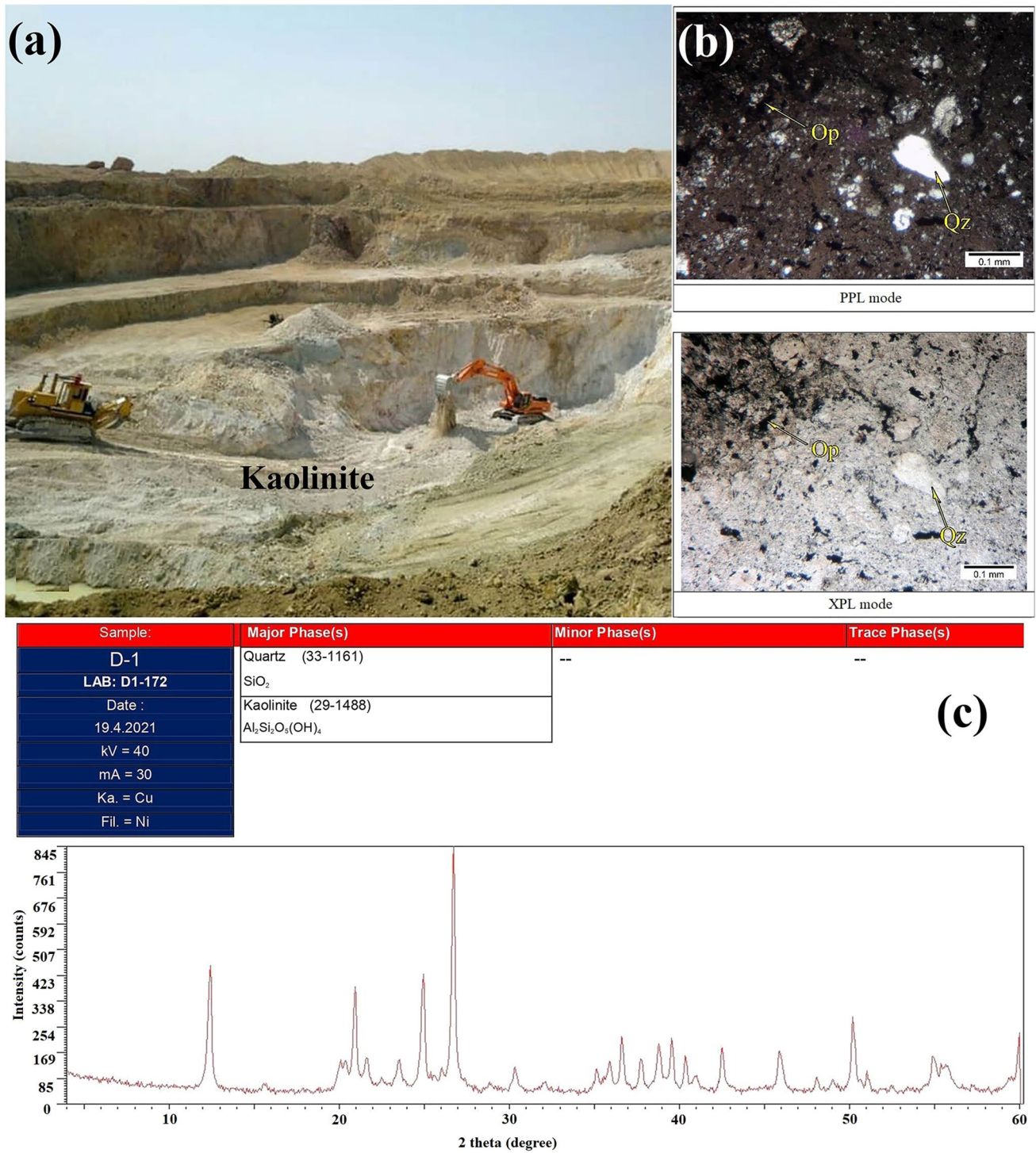


Fig. 14 a A kaolinite mine in zone F, b Thin section shows quartz (Qz) and opaque (Op) minerals, c Result of XRD analysis

faults and fractures on a regional scale. Usually, a fault buffer map is used as an evidential layer. Applying PF analysis for preparing the geological structures layer could be a better idea. In PF analysis, some vital parameters of fractures such as fracture numbers, fracture lengths, and fracture intersections are assumed to avoid a raw

evaluation of fractures. It is recommended to employ the map of the intersection of faults and intrusive contacts for creating the ultimate geological structures. These intersection points can reveal appropriate locations for specifying mineralized zones. At the regional scale, the application of stream sediment geochemistry data can be helpful if the

results are interpreted considering the lithology. Elementary maps can be converted into fuzzy layouts using the fuzzy OR operator. Stream sediment geochemistry provides helpful information about the distribution of elements in regional scale studies. In far and inaccessible districts such as the FGBB, stream sediment geochemistry can be performed to create the geochemistry layer due to its high coverage. Data integration using fuzzy logic resulted in the defining seven favorable zones in FGBB. Anomaly checking was conducted using field and laboratory studies to ensure the accuracy of the results. At last, Zones A, B, and C were recommended for further investigation due to promising field evidence, geochemistry anomalies, severe phyllic and argillic alterations, and dominant structural features.

**Acknowledgements** Golgohar Mining and Industrial Company (GEG) is sincerely appreciated and thanked for its financial and spiritual support. Institute of Science and High Technology and Environmental Sciences, Graduate University of Advanced Technology is thanked for providing the spectroradiometer.

**Author Contributions** Conceptualization: MH, Methodology: MH; ZAL; MHZ; Formal analysis and investigation: ZAL; Writing—original draft preparation: HS; Writing—review and editing: HS; MH, Resources: MH; ZAL; Supervision: MHZ; HS.

**Funding** This research received no external funding.

## Declarations

**Conflicts of interest** The authors declared that they have no conflict of interest.

## References

- Abrams, M., & Yamaguchi, Y. (2019). Twenty years of ASTER contributions to lithologic mapping and mineral exploration. *Remote Sensing*, 11(11), 1394. <https://doi.org/10.3390/rs11111394>
- Adiri, Z., Lhissou, R., El Harti, A., Jellouli, A., & Chakouri, M. (2020). Recent advances in the use of public domain satellite imagery for mineral exploration: A review of Landsat-8 and Sentinel-2 applications. *Ore Geology Reviews*, 117, 103332. <https://doi.org/10.1016/j.oregeorev.2020.103332>
- Aghanabati, A. (2006). Geology of Iran. Ministry of industry & mine geological survey of Iran.
- Behera, S., & Panigrahi, M. K. (2021). Mineral prospectivity modeling using singularity mapping and multifractal analysis of stream sediment geochemical data from the auriferous Hutti–Maski schist belt, S. India. *Ore Geology Reviews*, 131, 104029. <https://doi.org/10.1016/j.oregeorev.2021.104029>
- Bonham-Carter, G. F. (1994). *Geographic information systems for geoscientists: Modelling with GIS* (p. 398p). Pergamon.
- Borovec, Z. (1996). Evaluation of the concentrations of trace elements in stream sediments by factor and cluster analysis and the sequential extraction procedure. *Science of the Total Environment*, 177(1–3), 237–250. [https://doi.org/10.1016/0048-9697\(95\)04901-0](https://doi.org/10.1016/0048-9697(95)04901-0)
- Carranza, E. J. M., & Hale, M. (1997). A catchment basin approach to the analysis of geochemical-geological data from Albay province, Philippines. *Journal of Geochemical Exploration*, 60, 157–171. [https://doi.org/10.1016/S0375-6742\(97\)00032-0](https://doi.org/10.1016/S0375-6742(97)00032-0)
- Carranza, E. J. M., & Hale, M. (2001). Geologically Constrained Fuzzy Mapping of Gold Mineralization Potential, Baguio District, Philippines. *Natural Resources Research*, 10, 125–136. <https://doi.org/10.1023/A:1011500826411>
- Carranza, E. J. M. (2008). *Geochemical anomaly and mineral prospectivity mapping in GIS, Handbook of exploration and environmental geochemistry* (Vol. 11). Elsevier.
- Carranza, E. J. M. (2017). Natural resources research publications on geochemical anomaly and mineral potential mapping, and introduction to the special issue of papers in these fields. *Natural Resources Research*, 26(4), 379–410. <https://doi.org/10.1007/s11053-017-9348-1>
- Carranza, E. J. M. (2021). Fuzzy modeling of surficial uranium prospectivity in British Columbia (Canada) with a weighted fuzzy algebraic sum operator. *Journal of Earth Science*, 32(2), 293–309. <https://doi.org/10.1007/s11053-005-4674-0>
- Chiprés, J. A., Castro-Larragoitia, J., & Monroy, M. G. (2009). Exploratory and spatial data analysis (EDA–SDA) for determining regional background levels and anomalies of potentially toxic elements in soils from Catorce–Matehuala, Mexico. *Applied Geochemistry*, 24, 1579–1589. <https://doi.org/10.1016/j.apgeochem.2009.04.022>
- Drusch, M., Del Bello, U., Carlier, S., Colin, O., Fernandez, V., Gascon, F., & Bargellini, P. (2012). Sentinel-2: ESA’s optical high-resolution mission for GMES operational services. *Remote Sensing of Environment*, 120, 25–36. <https://doi.org/10.1016/j.rse.2011.11.026>
- Esmailoghli, S., Tabatabaei, S. H., & Carranza, E. J. M. (2021). Spatio-geologically informed fuzzy classification: An innovative method for recognition of mineralization-related patterns by integration of elemental, 3d spatial, and geological information. *Natural Resources Research*, 30(2), 989–1010. <https://doi.org/10.1007/s11053-020-09798-x>
- Ford, A., Miller, J. M., & Mol, A. G. (2016). A comparative analysis of weights of evidence, evidential belief functions, and fuzzy logic for mineral potential mapping using incomplete data at the scale of investigation. *Natural Resources Research*, 25(1), 19–33. <https://doi.org/10.1007/s11053-015-9263-2>
- Ghasemzadeh, S., Maghsoudi, A., Yousefi, M., & Mihalasky, M. J. (2019). Stream sediment geochemical data analysis for district-scale mineral exploration targeting: Measuring the performance of the spatial U-statistic and CA fractal modeling. *Ore Geology Reviews*, 113, 103115. <https://doi.org/10.1016/j.oregeorev.2019.103115>
- Ghezlbash, R., Maghsoudi, A., Bigdeli, A., & Carranza, E. J. M. (2021). Regional-scale mineral prospectivity mapping: Support vector machines and an improved data-driven multi-criteria decision-making technique. *Natural Resources Research*, 30(3), 1977–2005. <https://doi.org/10.1007/s11053-021-09842-4>
- Goetz, A. F., Rock, B. N., & Rowan, L. C. (1983). Remote sensing for exploration; An overview. *Economic Geology*, 78(4), 573–590. <https://doi.org/10.2113/gsecongeo.78.4.573>
- Gupta, R. P. (2003). *Remote Sensing Geology* (2nd ed., p. 656). Springer.
- Hardcastle, K. C., Emery, J. M., Tinkham, D. J., & Brooks, J. A. (1997). Photolineament Factor Analysis: A new computerized method of remotely assessing the degree to which bedrock is fractured, NWWA Conf. Innov. Ground Water Tech. of the 90’s.
- Hardcastle, K. C. (1995). Photolineament factor: A new computer-aided method for remotely sensing the degree to which bedrock is fractured. *Photogrammetric Engineering and Remote Sensing*, 61(6), 739–746.
- Helvoort, P. J., Filzmoser, P., & van Gaans, P. F. (2005). Sequential factor analysis as a new approach to multivariate analysis of

- heterogeneous geochemical datasets: An application to a bulk chemical characterization of fluvial deposits (Rhine–Meuse delta, The Netherlands). *Applied Geochemistry*, 20(12), 2233–2251. <https://doi.org/10.1016/j.apgeochem.2005.08.009>
- Hubbard, B. E., & Crowley, J. K. (2005). Mineral mapping on the Chilean-Bolivian Altiplano using Co-Orbital ALI, ASTER and Hyperion imagery: Data dimensionality issues and solutions. *Remote Sensing of Environment*, 99, 173–186. <https://doi.org/10.1016/j.rse.2005.04.027>
- Hunt, G. R. (1977). Spectral signatures of particulate minerals in the visible and near infrared. *Geophysics*, 42, 501–513. <https://doi.org/10.1190/1.1440721>
- Hunt, G. R., & Ashley, R. P. (1979). Spectra of altered rocks in the visible and near infrared. *Economic Geology*, 74, 1613–1629. <https://doi.org/10.2113/gsecongeo.74.7.1613>
- Jung, D., Keller, J., Khorasani, R., Marcks, C., & Baumann, A. (1983). Petrology of the Tertiary magmatic activity in the northern Lut area east of Iran. *Neues Jahrbuch für Geologie und Paläontologie Abhandlungen*. <https://doi.org/10.1127/njgpa/168/1984/417>
- Kashani, S. B. M., Abedi, M., & Norouzi, G. H. (2016). Fuzzy logic mineral potential mapping for copper exploration using multi-disciplinary geo-datasets, a case study in seridune deposit, Iran. *Earth Science Informatics*, 9(2), 167–181. <https://doi.org/10.1007/s12145-015-0246-y>
- Kruse, F. A., Lefkoff, A. B., Boardman, J. W., Heidebrecht, K. B., Shapiro, A. T., Barloon, P. J., & Goetz, A. F. H. (1993). The spectral image processing system (SIPS)—interactive visualization and analysis of imaging spectrometer data. *Remote Sensing of Environment*, 44(2–3), 145–163. [https://doi.org/10.1016/0034-4257\(93\)90013-N](https://doi.org/10.1016/0034-4257(93)90013-N)
- Legg, C. (1994). *Remote sensing and geographical information systems: geological mapping, mineral exploration and mining*. Ellis Horwood Ltd.
- Lyon, R. J. P., & Lee, K. (1970). Remote sensing in exploration for mineral deposits. *Economic Geology*, 65(7), 785–800. <https://doi.org/10.2113/gsecongeo.65.7.785>
- Mahanta, P., & Maiti, S. (2018). Regional scale demarcation of alteration zone using ASTER imageries in South Purulia Shear Zone, East India: Implication for mineral exploration in vegetated regions. *Ore Geology Reviews*, 102, 846–861. <https://doi.org/10.1016/j.oregeorev.2018.07.028>
- Manuel, R., Brito, M. D. G., Chichorro, M., & Rosa, C. (2017). Remote sensing for mineral exploration in central Portugal. *Minerals*, 7(10), 184. <https://doi.org/10.3390/min7100184>
- Moradpour, H., Rostami Paydar, G., Feizizadeh, B., Blaschke, T., Pour, A. B., Valizadeh Kamran, K., & Hossain, M. S. (2021). Fusion of ASTER satellite imagery, geochemical and geology data for gold prospecting in the Astaneh granite intrusive, West Central Iran. *International Journal of Image and Data Fusion*. <https://doi.org/10.1080/19479832.2021.1915395>
- Noori, L., Pour, A. B., Askari, G., Taghipour, N., Pradhan, B., Lee, C. W., & Honarmand, M. (2019). Comparison of different algorithms to map hydrothermal alteration zones using ASTER remote sensing data for polymetallic vein-type ore exploration: Toroud-Chahshirin Magmatic Belt (TCMB), North Iran. *Remote Sensing*, 11(5), 495. <https://doi.org/10.3390/rs11050495>
- Nykänen, V., Groves, D. I., Ojala, V. J., Eilu, P., & Gardoll, S. J. (2008). Reconnaissance-scale conceptual fuzzy-logic prospectivity modelling for iron oxide copper–gold deposits in the northern Fennoscandian Shield, Finland. *Australian Journal of Earth Sciences*, 55(1), 25–38. <https://doi.org/10.1080/08120090701581372>
- Pahlavani, P., Riahi, S., & Bigdeli, B. (2020). Ranking potentially favorable mineralization zones using fuzzy VIKOR vs. Dempster-Shafer-fuzzy AHP methods, a case study: South-east of the Sarcheshmeh copper mine, Kerman, Iran. *Arabian Journal of Geosciences*, 13(21), 1–21. <https://doi.org/10.1007/s12517-020-06145-5>
- Phillis, Y. A., & Andriantiatsaholainaina, L. A. (2001). Sustainability: An ill-defined concept and its assessment using fuzzy logic. *Ecological Economics*, 37(3), 435–456. [https://doi.org/10.1016/S0921-8009\(00\)00290-1](https://doi.org/10.1016/S0921-8009(00)00290-1)
- Ranasinghe, P. N., Fernando, G. W. A. R., Dissanayake, C. B., & Rupasinghe, M. S. (2008). Stream sediment geochemistry of the upper Mahaweli River Basin of Sri Lanka—Geological and environmental significance. *Journal of Geochemical Exploration*, 99(1–3), 1–28. <https://doi.org/10.1016/j.gexplo.2008.02.001>
- Reimann, C., Filzmoser, P., & Garrett, R. G. (2002). Factor analysis applied to regional geochemical data: Problems and possibilities. *Applied Geochemistry*, 17, 185–206. [https://doi.org/10.1016/S0883-2927\(01\)00066-X](https://doi.org/10.1016/S0883-2927(01)00066-X)
- Roonwal, G. S. (2018). Remote Sensing in Mineral Exploration. *Mineral Exploration* (pp. 119–153). Singapore: Practical Application Springer. [https://doi.org/10.1007/978-981-10-5604-8\\_4](https://doi.org/10.1007/978-981-10-5604-8_4)
- Saadati, H., Afzal, P., Torshizian, H., & Solgi, A. (2020). Geochemical exploration for lithium in NE Iran using the geochemical mapping prospectivity index, staged factor analysis, and a fractal model Geochemistry. *Exploration Environment Analysis*, 20(4), 461–472. <https://doi.org/10.1144/geochem2020-020>
- Sabine, C. (1999). Remote sensing strategies for mineral exploration. *Remote Sensing for the Earth Sciences—Manual of Remote Sensing*, 375–447.
- Sadeghi, M., Billay, A., & Carranza, E. J. M. (2015). Analysis and mapping of soil geochemical anomalies: Implications for bed-rock mapping and gold exploration in Giyani area, South Africa. *Journal of Geochemical Exploration*, 154, 180–193. <https://doi.org/10.1016/j.gexplo.2014.11.018>
- Sekandari, M., Masoumi, I., Pour, A. B., Muslim, A. M., Hossain, M. S., & Misra, A. (2020). ASTER and WorldView-3 satellite data for mapping lithology and alteration minerals associated with Pb-Zn mineralization. *Geocarto International*. <https://doi.org/10.1080/10106049.2020.1790676>
- Tarkian, M., Lotfi, M., & Baumann, A. (1983). Tectonic, magmatism and the formation of mineral deposits in the central Lut, east Iran. *Earth sciences*, 51, 357–383.
- Tarkian, M., Lotfi, M., & Baumann, A. (1984). Magmatic copper and lead-zinc ore deposits in the Central Lut, East Iran. *Neues Jahrbuch für Geologie und Paläontologie-Abhandlungen*. <https://doi.org/10.1127/njgpa/168/1984/497>
- Toutin, T. (2004). Comparison of stereo-extracted DTM from different high-resolution sensors: SPOT-5, EROS-A, IKONOS-II, and QuickBird. *IEEE Transactions on Geoscience and Remote Sensing*, 42(10), 2121–2129. <https://doi.org/10.1109/TGRS.2004.834641>
- Wambo, J. D. T., Pour, A. B., Ganno, S., Asimow, P. D., Zoheir, B., dos Reis Salles, R., & Muslim, A. M. (2020). Identifying high potential zones of gold mineralization in a sub-tropical region using Landsat-8 and ASTER remote sensing data: A case study of the Ngoura-Colomines goldfield, eastern Cameroon. *Ore Geology Reviews*, 122, 103530. <https://doi.org/10.1016/j.oregeorev.2020.103530>
- Yang, L., Wang, Q., & Liu, X. (2015). Correlation between mineralization intensity and fluid–rock reaction in the Xinli gold deposit, Jiaodong Peninsula, China: Constraints from petrographic and statistical approaches. *Ore Geology Review*, 71, 29–39. <https://doi.org/10.1016/j.oregeorev.2015.04.005>
- Yousefi, M., Kamkar-Rouhani, A., & Carranza, E. J. M. (2012). Geochemical mineralization probability index (GMPI): A new approach to generate enhanced stream sediment geochemical evidential map for increasing probability of success in mineral potential mapping. *Journal of Geochemical Exploration*, 115, 24–35. <https://doi.org/10.1016/j.gexplo.2012.02.002>

- Yousefi, M., Carranza, E. J. M., & Kamkar-Rouhani, A. (2013). Weighted drainage catchment basin mapping of geochemical anomalies using stream sediment data for mineral potential modeling. *Journal of Geochemical Exploration*, 128, 88–96. <https://doi.org/10.1016/j.gexplo.2013.01.013>
- Yousefi, M., Kamkar-Rouhani, A., & Carranza, E. J. M. (2014). Application of staged factor analysis and logistic function to create a fuzzy stream sediment geochemical evidence layer for mineral prospectivity mapping. *Geochemistry Exploration, Environment, Analysis*, 14(1), 45–58. <https://doi.org/10.1144/geochem2012-144>
- Yousefi, M., & Carranza, E. J. M. (2017). Union score and fuzzy logic mineral prospectivity mapping using discretized and continuous spatial evidence values. *Journal of African Earth Sciences*, 128, 47–60. <https://doi.org/10.1016/j.jafrearsci.2016.04.019>
- Yousefi, M., Carranza, E. J. M., Kreuzer, O. P., Nykänen, V., Hronsky, J. M., & Mihalasky, M. J. (2021). Data analysis methods for prospectivity modelling as applied to mineral exploration targeting: State-of-the-art and outlook. *Journal of Geochemical Exploration*. <https://doi.org/10.1016/j.gexplo.2021.106839>
- Yousefi, M., & Hronsky, J. M. (2023). Translation of the function of hydrothermal mineralization-related focused fluid flux into a mappable exploration criterion for mineral exploration targeting. *Applied Geochemistry*, 149, 105561. <https://doi.org/10.1016/j.apgeochem.2023.105561>
- Zuluaga, M. C., Norini, G., Lima, A., Albanese, S., David, C. P., & De Vivo, B. (2017). Stream sediment geochemical mapping of the Mount Pinatubo-Dizon Mine area, the Philippines: Implications for mineral exploration and environmental risk. *Journal of Geochemical Exploration*, 175, 18–35. <https://doi.org/10.1016/j.gexplo.2016.12.012>

**Publisher's Note** Springer Nature remains neutral with regard to jurisdictional claims in published maps and institutional affiliations.

Springer Nature or its licensor (e.g. a society or other partner) holds exclusive rights to this article under a publishing agreement with the author(s) or other rightsholder(s); author self-archiving of the accepted manuscript version of this article is solely governed by the terms of such publishing agreement and applicable law.